High-power single transverse and polarization mode VCSEL for silicon photonics integration

Research Article | Vol. 27, No. 13 | 24 Jun 2019 | OPTICS EXPRESS 18892
Optics EXPRESS

High-power single transverse and polarization mode VCSEL for silicon photonics integration

ERIK HAGLUND,[1,2] MEHDI JAHED,[1] JOHAN S. GUSTAVSSON,[1] ANDERS LARSSON,[1,*] JEROEN GOYVAERTS,[3] ROEL BAETS,[3] GUNTHER ROELKENS,[3] MARC RENSING,[4] AND PETER O'BRIEN[4]

[1]*Photonics Laboratory, Department of Microtechnology and Nanoscience, Chalmers University of Technology, SE-412 96 Göteborg, Sweden*
[2]*Currently with OptiGOT AB, SE-411 33 Göteborg, Sweden*
[3]*Photonics Research Group, Ghent University-imec, Technologiepark-Zwijnaarde 126, 9052 Ghent, Belgium*
[4]*Tyndall National Institute, Cork, Ireland*
**anders.larsson@chalmers.se*

Abstract: We demonstrate a 6.5 mW single transverse and polarization mode GaAs-based oxide-confined VCSEL at 850 nm. High power is enabled by a relatively large oxide aperture and an epitaxial design for low resistance, low optical loss, and high slope efficiency VCSELs. With the oxide aperture supporting multiple polarization unrestrained transverse modes, single transverse and polarization mode operation is achieved by a transverse and polarization mode filter etched into the surface of the VCSEL. While the VCSEL is specifically designed for light source integration on a silicon photonic integrated circuit, its performance in terms of power, spectral purity, polarization, and beam properties are of great interest for a large range of applications.

1. Introduction

Among the various techniques for light source integration on silicon photonic integrated circuits (Si-PICs) [1], flip-chip integration of a tilted vertical-cavity surface-emitting laser (VCSEL) over a grating coupler, Fig. 1, offers certain advantages [2,3]. The VCSEL itself has the power efficiency and small footprint needed for dense integration. The integration technique enables independent optimization of VCSEL performance, eliminates optical feedback to the VCSEL, and facilitates unidirectional coupling without resorting to more complex grating couplers [4] or optical designs [5] needed for normal incidence.

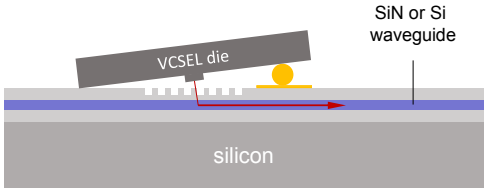

Fig. 1. Flip-chip integration of a VCSEL die at an angle over a grating coupler on a silicon photonic integrated circuit.

With the Si or silicon nitride (SiN) waveguides used in Si-PICs being single-mode and with the grating couplers being polarization sensitive, the VCSEL has to be single (fundamental) transverse mode with a stable and linear state of polarization. Because of optical losses in various parts of the Si-PIC (grating couplers, splitters, multiplexers, etc.) a high output power from the VCSEL is also desired to facilitate a practical power budget.

In this paper we report on an 850 nm single transverse and polarization mode VCSEL for tilted flip-chip integration over a grating coupler on a Si-PIC with SiN waveguides. The

#365521 https://doi.org/10.1364/OE.27.018892
Journal © 2019 Received 18 Apr 2019; revised 5 Jun 2019; accepted 7 Jun 2019; published 20 Jun 2019

Optics EXPRESS

VCSEL emits a record 6.5 mW of single transverse and polarization mode power with >30 dB suppression of higher order transverse modes and >20 dB suppression of the orthogonal polarization state. The VCSEL is intended for light source integration on a short-wavelength sensor PIC being developed in the European project PIX4life [6]. The PIC is based on a silicon-nitride waveguide platform on silicon where the SiN waveguides are transparent at the very-near infrared and visible wavelengths (loss <1.0 dB/cm) needed in many life science applications [7]. Previous work on high-power single-mode VCSELs (no polarization control) include a bottom-emitting 960 nm VCSEL that is single-mode at high currents with up to 15 mW of output power [8].

The concept used is that of a GaAs-based oxide-confined VCSEL with a relatively large oxide aperture and a transverse and polarization mode filter etched into the surface, Fig. 2 [9]. The large oxide aperture enables low resistance for delayed thermal rollover and high output power but supports multiple transverse modes. The mode filter is a sub-wavelength grating etched in an area with a diameter less than the diameter of the oxide aperture. With the sub-wavelength grating acting as an effective index medium with a polarization dependent effective index, its spatial extent (diameter relative the diameter of the oxide aperture) controls the transverse mode selectivity while the orientation of the grating lines provides polarization mode selectivity. The sub-wavelength grating pitch, in contrast to a pitch larger than the wavelength, also avoids excessive optical loss and beam degradation due to diffraction.

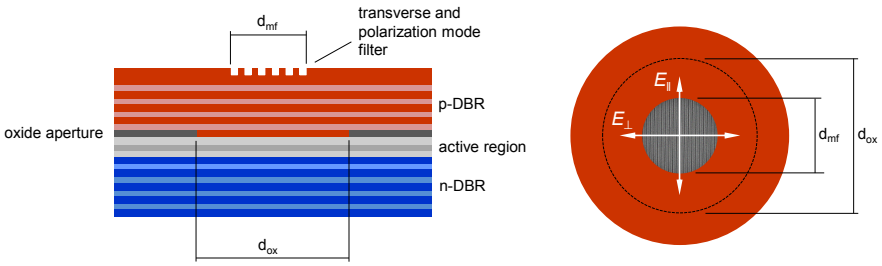

Fig. 2. The oxide-confined VCSEL with a transverse and polarization mode filter etched into the surface. The diameters of the oxide aperture (d_{ox}) and the mode filter (d_{mf}) are indicated and the two orthogonal polarization states ($E_\perp$ and $E_\parallel$) are defined. Left: side view. Right: top view.

2. VCSEL design and fabrication

The epitaxial structure, grown by metal-organic chemical-vapor epitaxy on a GaAs substrate, consists of an active region with strained InGaAs/AlGaAs quantum wells (QWs) sandwiched between a lower n-type AlGaAs distributed Bragg reflector (DBR) and an upper p-type AlGaAs DBR with 29 and 21 pairs, respectively. Both DBRs have graded composition interfaces and are modulation doped for low resistance and low optical loss. A high-Al content layer positioned above the active region is used for the formation of an oxide aperture for transverse optical and current confinement.

The optical thickness of the uppermost layer of the top DBR is increased from a quarter wavelength to half a wavelength, which serves to reduce the reflectance of that DBR through an anti-phase reflection at the semiconductor-air interface. Thinning of this layer increases the reflectance until it reaches a maximum value when the thickness is a quarter wavelength. Local etching results in a spatially dependent mirror reflectance, which is used for transverse mode discrimination, while an anisotropic structure (grating) results in a polarization dependent reflectance used for polarization mode discrimination [10].

The mode discrimination imposed by the mode filter was studied using an effective index model [11] where the longitudinal and transverse dependencies of the modal optical fields are separated. The longitudinal variation of the field is computed from an eigenvalue equation, where the real and imaginary part of the eigenvalue are related to a cavity effective index and

Optics EXPRESS

cavity loss, respectively. This is done for all separate transverse regions. The results are then input to another eigenvalue equation for the transverse variation of the field. The real and imaginary part of this eigenvalue are related to the modal wavelength and modal loss, respectively. Because of the pitch of the grating being much smaller than the wavelength, the grating was treated as an effective index medium [10] with the effective indices for light polarized parallel and perpendicular to the grating lines being different. In the following, light polarized perpendicular (parallel) to the grating lines is denoted by $E_{\perp}$ ($E_{\parallel}$), see Fig. 2.

The VCSEL is designed for fundamental transverse mode (LP01) operation with $E_{\perp}$ polarization. Varying the design parameters in the simulations indicated that an oxide aperture diameter close to 5 μm and a mode filter diameter close to 3 μm would provide maximum transverse mode selectivity when the grating pitch, depth, and fill-factor is 120 nm, 59 nm, and 55%, respectively. The fill-factor is defined as the ratio between the width of the grating tooth and the pitch. Figure 3(a) shows the dependence of threshold gain for the LP01-$E_{\perp}$ and LP11-$E_{\perp}$ modes on the mode filter (grating) diameter, with the diameter of the oxide aperture being 5 μm. At a mode filter diameter of 3 μm, the threshold gain for the LP01-$E_{\perp}$ mode is about 2000 cm^{-1}, which should allow for a low threshold current. Figure 3(b) shows the dependence of transverse and polarization mode selectivity on the mode filter diameter, with the diameter of the oxide aperture again being 5 μm. Polarization mode selectivity is quantified as the difference in threshold gain between the LP01-$E_{\parallel}$ and LP01-$E_{\perp}$ modes. At a mode filter diameter of 3 μm, the polarization mode selectivity is 270 cm^{-1}, which is sufficient for strong suppression of the LP01-$E_{\parallel}$ mode because of the near-identical transverse intensity distributions of the two orthogonally polarized LP01 modes [12]. Transverse mode selectivity is quantified as the difference in threshold gain between the first higher order transverse LP11 mode (both LP11-$E_{\perp}$ and LP11-$E_{\parallel}$) and the fundamental LP01-$E_{\perp}$ mode. At the optimum mode filter diameter of 3 μm, the transverse mode selectivity is around 1000 cm^{-1}, which should result in strong suppression of both polarization states of the LP11 mode. In all calculations, the threshold gain is defined as the material gain in the QWs at threshold.

Figure 3(a) shows the high resonator loss when the half wavelength thick top layer covers the entire VCSEL (mode filter diameter = 0). It also shows the low resonator loss when the thickness of the entire top layer is reduced to a quarter wavelength (mode filter diameter much larger than the oxide aperture diameter). In between, the resonator loss is reduced with increasing filter diameter since the overlap of the modes with the high loss (unetched) region is reduced. The difference in the rate at which the loss decreases with increasing filter diameter for the modes, caused by the difference in their transverse intensity ditributions, results in maximum mode discrimination at a filter diameter of 3 μm, Fig. 3(b). See [9] for details.

In a similar fashion, Fig. 4 shows the dependencies of threshold gain and threshold gain differences on the grating fill-factor with the diameters of the oxide aperture and the mode filter set to 5 and 3 μm, respectively, and the grating pitch and depth set to 120 and 59 nm, respectively. The threshold gain for the fundamental transverse LP01-$E_{\perp}$ mode depends only weakly on the grating fill-factor. Largest polarization mode discrimination (LP01-$E_{\parallel}$ vs. LP01-$E_{\perp}$) is observed for fill-factors of 80-90%. The threshold gain difference for the higher order transverse LP11 mode (~1000 cm^{-1}) is largely independent on the grating fill-factor.

Optics EXPRESS

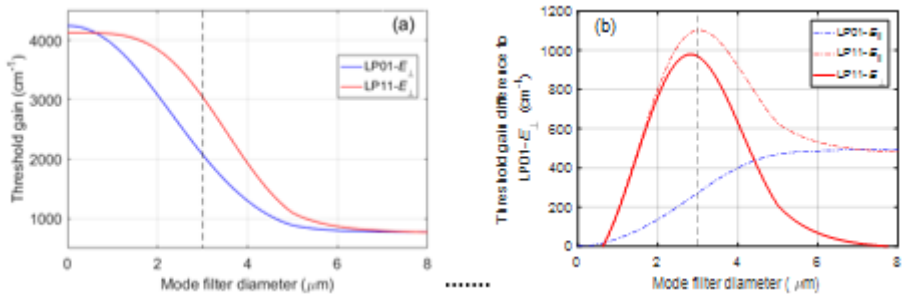

Fig. 3. Dependence of a) threshold gain for the transverse LP01-$E_{\perp}$ and LP11-$E_{\perp}$ modes and b) transverse and polarization mode discrimination (threshold gain differences) on mode filter (grating) diameter. The grating pitch, depth, and fill-factor is 120 nm, 59 nm, and 55%, respectively. The diameter of the oxide aperture is 5 μm.

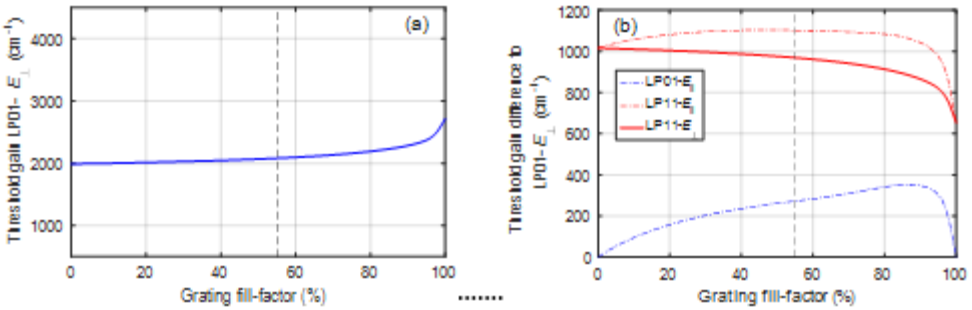

Fig. 4. Dependence of a) threshold gain for the fundamental transverse LP01-$E_{\perp}$ mode and b) transverse and polarization mode discrimination (threshold gain differences) on grating fill-factor. The grating pitch and depth is 120 and 59 nm, respectively, and the oxide aperture and mode filter diameters are 5 and 3 μm, respectively.

VCSELs were fabricated using standard techniques for mesa etching, selective oxidation, and contact and pad metallization. Both contact pads are on the top surface to enable flip-chip integration, Fig. 5. The sub-wavelength grating was defined early in the fabrication using electron beam lithography and metal alignment marks. A precise grating etch depth was achieved using a calibrated Ar-ion milling process, Fig. 6. The same alignment marks were later used to define the VCSEL mesa by electron beam lithography. This enables proper alignment of the oxide aperture and the mode filter.

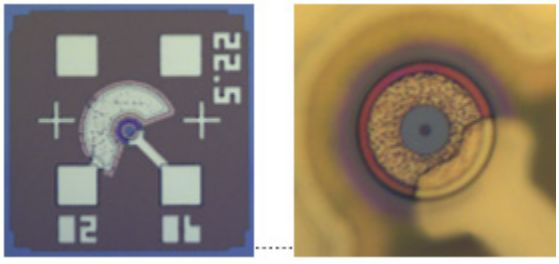

Fig. 5. Microscope images of the VCSEL. Left: the VCSEL die with n- and p-contact pads on the top surface for flip-chip integration. Right: magnified image with the mode filter visible in the center of the optical aperture.

Optics EXPRESS

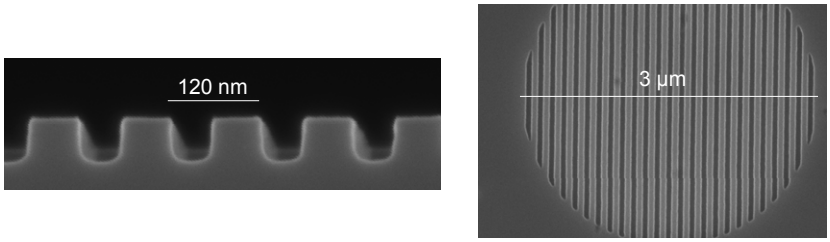

Fig. 6. Scanning electron microscope images of a sub-wavelength surface grating with 120 nm pitch, 59 nm depth, and 55% fill-factor. Left: cross-sectional view. Right: top view.

3. VCSEL performance

The performance shown below is for a VCSEL with the following parameters defining the critical dimensions: oxide aperture diameter = 5 µm, mode filter diameter = 3 µm, grating pitch = 120 nm, grating depth = 59 nm, and grating fill-factor = 55%. Note that the grating fill-factor is less than that providing the highest polarization mode selectivity (80-90%), Fig. 4(b). This is because the grating fabrication process produces the highest quality grating when the fill-factor is around 50%. However, at a fill-factor of 55% the polarization mode selectivity is still very high, with 270 cm^{-1} of threshold gain difference, Fig. 4(b).

Figure 7 shows the measured output power and voltage as a function of current with a collimating anti-reflection coated lens positioned between the VCSEL and a calibrated large-area detector. With a threshold current of 0.4 mA and a slope efficiency as high as 1.2 W/A, the power reaches a maximum of 6.5 mW at thermal rollover. The differential resistance at the mid-point is just above 100 Ω.

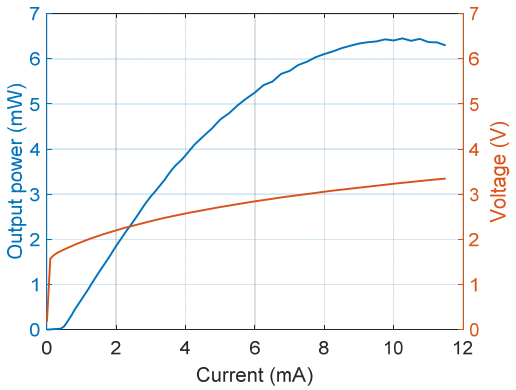

Fig. 7. Output power and voltage as a function of current with power measured without a polarizer.

Polarization resolved measurements of output power vs. current were performed by inserting a polarizer between the collimating lens and the detector. The results are shown in Fig. 8. At bias currents above 4 mA, the orthogonal polarization suppression ratio (OPSR) exceeds 20 dB with polarization perpendicular to the grating lines as expected from the simulations, Fig. 4(b). Compared to Fig. 7, it is seen that some power is lost when inserting the polarizer.

Optics EXPRESS

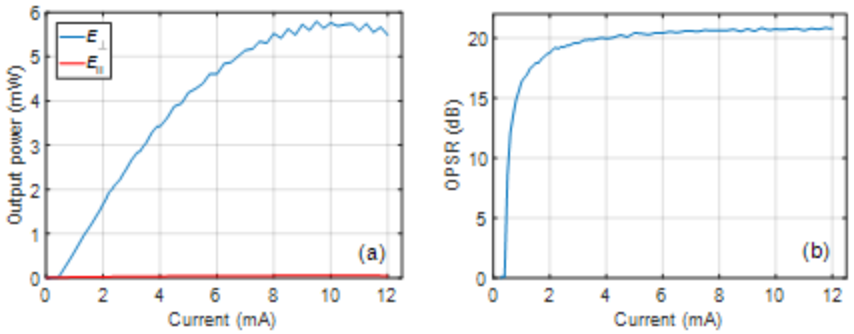

Fig. 8. a) Output power in the two orthogonal polarization states as a function of current, measured with a polarizer between the VCSEL and the photodiode. b) Orthogonal polarization mode suppression (OPSR) as a function of current.

Results from spectral measurements with the VCSEL coupled to an OM4 fiber using an anti-reflection coated lens system are shown in Fig. 9(a). The resolution of the optical spectrum analyzer was set to 0.01 nm. Fundamental transverse mode operation is evident with a suppression of higher order transverse modes exceeding 30 dB at currents above 1 mA, Fig. 9(b).

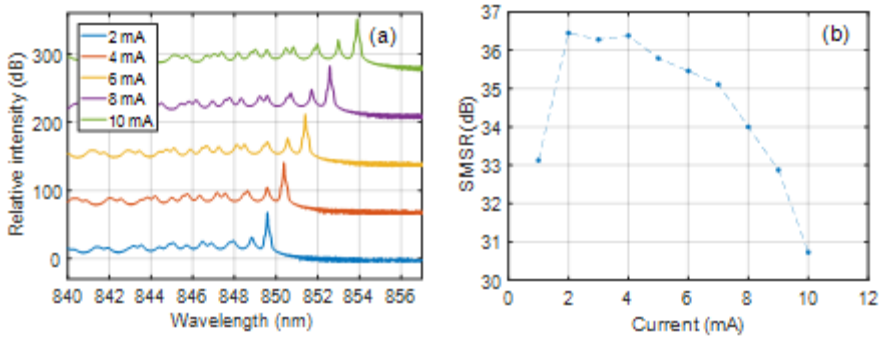

Fig. 9. a) Spectra at different currents from threshold to rollover. b) Higher order transverse mode suppression (side-mode suppression ratio, SMSR) as a function of current.

Figure 10 shows the red-shift of the wavelength of the fundamental transverse mode with current, Fig. 10(a), and dissipated power, Fig. 10(b). This is of importance for e.g. sensing applications where the wavelength is tuned by current. The super-linear dependence of wavelength on current is due to resistive loss being the dominant loss mechanism. The linear dependence on dissipated power is as expected from the linear dependence of the cavity resonance wavelength on temperature. From this data the thermal impedance was calculated to be 3.0 K/mW.

Optics EXPRESS

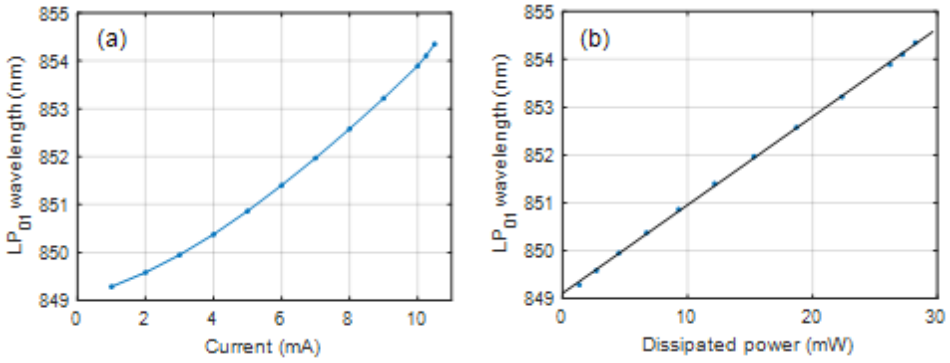

Fig. 10. Wavelength of the fundamental transverse LP01-$E_{\perp}$ mode as a function of a) current and b) dissipated power.

Finally, beam profiles were recorded by scanning a photodiode with a pin-hole in the polar plane at a distance of ~30 cm from the VCSEL. Figure 11 shows beam profiles recorded along directions perpendicular and parallel to the grating lines at different currents. The circular near-Gaussian beam has a $1/e^2$ full-width increasing from 15° at 2 mA to 16° at 10 mA, with a corresponding full-width at half maximum (FWHM) of 9° and 10°, respectively. The slight increase of beam divergence is caused by thermal lensing. The oscillations observed in the tails of the beam profiles are not caused by grating diffraction since they exist in both directions. We believe they are due to the circular mode filter together with a slight reduction of the resonator effective index in the filter region, creating an Airy pattern.

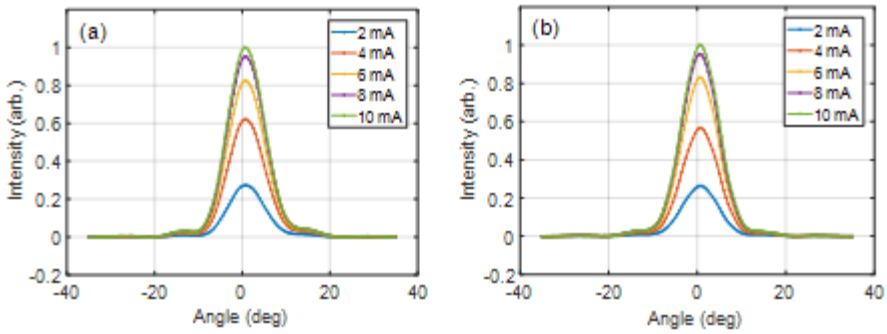

Fig. 11. Measured beam profile along directions perpendicular (a) and parallel (b) to the grating lines at different currents.

4. Summary and conclusions

In summary, we have demonstrated a single transverse and polarization mode 850 nm VCSEL with a record output power of 6.5 mW, >30 dB suppression of higher order transverse modes, >20 dB orthogonal polarization mode suppression, and a narrow FWHM beam divergence of 10°. The output power is more than 60% higher than previously achieved [9]. We conclude that mode filter integration is a powerful technique for controlling and tailoring the optical properties of GaAs-based oxide-confined VCSELs for a large range of applications.

Funding

European Union's Horizon 2020 research and innovation program (688519) (PIX4life); Swedish Research Council (2016-06077) (iTRAN); Swedish Foundation for Strategic Research (SE13-0014) (MuTOI).

Optics EXPRESS

References

1. Z. Wang, A. Abbasi, U. Dave, A. De Groote, S. Kumari, B. Kunert, C. Merckling, M. Pantouvaki, Y. Shi, B. Tian, K. Van Gasse, J. Verbist, R. Wang, W. Xie, J. Zhang, Y. Zhu, J. Bauwelinck, X. Yin, Z. Hens, J. Van Campenhout, B. Kuyken, R. Baets, G. Morthier, D. Van Thourhout, and G. Roelkens, "Novel light source integration approaches for silicon photonics," Laser Photonics Rev. **11**(4), 1700063 (2017).
2. H. Lu, J. S. Lee, Y. Zhao, C. Scarcella, P. Cardile, A. Daly, M. Ortsiefer, L. Carroll, and P. O'Brien, "Flip-chip integration of tilted VCSELs onto a silicon photonic integrated circuit," Opt. Express **24**(15), 16258–16266 (2016).
3. H. Lu, J.S. Lee, Y. Zhao, P. Cardile, A. Daly, L. Carroll, and P. O'Brien, "Hybrid integration of VCSELs onto a silicon photonic platform for biosensing application," Proc. SPIE **10072**, 100720K (2017).
4. B. Wang, J. Jiang, and G. Nordin, "Compact slanted grating couplers," Opt. Express **12**(15), 3313–3326 (2004).
5. K. S. Kaur, A. Z. Subramanian, P. Cardile, R. Verplancke, J. Van Kerrebrouck, S. Spiga, R. Meyer, J. Bauwelinck, R. Baets, and G. Van Steenberge, "Flip-chip assembly of VCSELs to silicon grating couplers via laser fabricated SU8 prisms," Opt. Express **23**(22), 28264–28270 (2015).
6. PIX4life. www.pix4life.eu
7. A. Z. Subramanian, P. Neutens, A. Dhakal, R. Jansen, T. Claes, X. Rottenberg, F. Peyskens, S. Selvaraja, P. Helin, B. Du Bois, K. Leyssens, S. Severi, P. Deshpande, R. Baets, and P. Van Dorpe, "Low-loss singlemode PECVD silicon nitride photonic wire waveguides for 532–900 nm wavelength window fabricated within a CMOS pilot line," IEEE Photonics J. **5**(6), 2202809 (2013).
8. S. A. Blokhin, N. A. Maleev, A. G. Kuzmenkov, J. A. Lott, M. M. Kulagina, Y. M. Zadiranov, A. G. Gladyshev, A. M. Nadtochiy, E. V. Nikitina, V. G. Tikhomirov, N. N. Ledentsov, and V. M. Ustinov, "Multi-mode to single-mode switching caused by self-heating in bottom-emitting intra-cavity contacted 960 nm VCSELs," Proc. SPIE **8276**, 82760W (2012).
9. Å. Haglund, J. S. Gustavsson, J. Bengtsson, P. Jedrasik, and A. Larsson, "Design and evaluation of fundamental-mode and polarization-stabilized VCSELs with a subwavelength surface grating," IEEE J. Quantum Electron. **42**(3), 231–240 (2006).
10. J. Gustavsson, A. Haglund, J. Vukusić, J. Bengtsson, P. Jedrasik, and A. Larsson, "Efficient and individually controllable mechanisms for mode and polarization selection in VCSELs, based on a common, localized, sub-wavelength surface grating," Opt. Express **13**(17), 6626–6634 (2005).
11. G. R. Hadley, "Effective index model for vertical-cavity surface-emitting lasers," Opt. Lett. **20**(13), 1483–1485 (1995).
12. P. Debernardi, J. M. Ostermann, M. Feneberg, C. Jalics, and R. Michalzik, "Reliable polarization control of VCSELs through monolithically integrated surface gratings: a comparative theoretical and experimental study," IEEE J. Sel. Top. Quantum Electron. **11**(1), 107–116 (2005).